Journal of Mining and Geology Vol. 60(1) 2024. pp. 113 - 128 0022-2763
© Nigerian Mining and Geosciences Society (NMGS) - Printed in Nigeria.
www.nmgs-journal.org

Provenance, Paleoclimate, Paleoenvironment and Kerogen Characterization of the Paleocene Imo Formation from Owan-1 Well: *Insights from Geochemistry and Mineralogy*

Jimoh, A.Y.[1], Ojo, O.J.[2], Haruna, K.A.[3] and Mariam, B.[1]

[1]Department of Geology and Mineral Science, Faculty of Pure and Applied Sciences, Kwara State University, PMB 1530, Malete, Nigeria.

[2]Department of Geology, Federal University Oye Ekiti, Oye-Ekiti, Nigeria.

[3]Department of Chemical and Geological Sciences, Al-Hikmah University, Ilorin, Nigeria.

Corresponding E-mail: yusuf.jimoh@kwasu.edu.ng

Abstract

The Paleocene shales of the Imo Formation, Niger Delta were investigated to reveal their organic and mineralogical composition, kerogen type, paleoweathering, provenance, paleoclimate, and paleoenvironments. Shale samples from Owan-1 well penetrating the Paleocene Imo Formation were analyzed by X-Ray Fluorescence (XRF), X-Ray Diffraction (XRD), and Fourier Transform Infra-red (FTIR) Spectroscopy. The results showed that the shales are enriched in SiO_2, Al_2O_3 and Fe_2O_3 compared to CaO, MgO, K_2O, MnO, TiO_2, and P_2O_5. The Average concentration of SiO_2, Al_2O_3 and Fe_2O_3 are 25.5 wt.%, 9.65 wt.% and 5.46 wt.% respectively. Bivariate plots of the Chemical Index of Alteration (CIA) vs Plagioclase Index of Alteration (PIA), and elemental ratio such as SiO_2/Al_2O_3 indicate low to moderate chemical weathering. The discriminant function diagram DF1 vs DF2, plots of TiO_2 vs Al_2O_3, and TiO_2 vs Zr revealed intermediate igneous provenance. The plot of SiO_2 vs (Al_2O_3+K_2O+Na_2O) indicates semi-humid to semi-arid climatic conditions. The high Sr/Ba indicates diagenesis and high salinity stratification in the water column. The Sr/Ba value >1 (avg. 1.27) suggests mainly marine depositional environments and oxic conditions for the shales. The main minerals identified by XRD are quartz and kaolinite with minor concentration of montmorillonite, chlorite, illite, biotite and carbonates. The spectra in the samples revealed bands within 1111cm^{-1}, 1102cm^{-1} and 1033cm^{-1} suggesting presence of quartz, kaolinite and illite. The FTIR spectra also showed presence of long chain aliphatic (saturated) compounds, unsaturated alkenyl C=C stretch, carbonyl C=O, hydroxyl compounds and aromatic phenolic group. The A and C factor from FTIR characterize the kerogen in the investigated shale samples as Type II with potential to generate oil and gas.

Keywords: *Diagenesis, Fluorescence, Kerogen, Paleoenvironment, Provenance, Shales*

Introduction

Scientists have extensively studied the formation of sedimentary rocks in different basins throughout time. Sediment deposition occurs under unique physical and chemical conditions that vary throughout geological periods. Examination of depositional settings may occur at both local and large geographical levels. There has been much research on the geochemistry of sedimentary rocks in unravelling the paleo-conditions, provenance, and paleotectonic settings; however, the specifics of each case are highly dependent on the type of source rock(s), the extent and duration of weathering, diagenesis, and the extent of sedimentary recycling (Nesbitt and Young, 1984; McLennan *et al.*, 1993). When studying paleoenvironmental conditions and hydrocarbon exploration/exploitation, it is essential to understand the origin and tectonic background of sedimentary basin-fills. The Niger Delta Basin and the adjoining Anambra basin of Nigeria are known for hydrocarbon deposits (Fig. 1), and several researchers have investigated the basins in terms of tectonic evolution and stratigraphy, including sequence stratigraphy, lithostratigraphy, biostratigraphy, age, paleoenvironments, and petroleum system (Bustin, 1988; Nwajide and Reijers, 1996; Adegoke *et al.*, 2015; Chudi *et al.*, 2016; Dim *et al.*, 2017; Edegbai *et al.*, 2019; Ogbe *et al.*, 2020; Ikegwuonu *et al.*, 2020; Ozumba and Dim, 2022; Aigbadon *et al.*, 2022; Omietimi *et al.*, 2022; Ejeh *et al.*, 2024). Most of the geological investigations on the Imo Formation have been on the surface samples mainly because of the scarcity of subsurface data and the attention given to the basin particularly the petroleum system. Hence, this research provides insights into the organic characterization, paleoweathering, provenance, tectonic setting, and paleoenvironmental reconstruction of the shale samples obtained from Owan-1 well through non-destructive analytical methods such as X-Ray Fluorescence (XRF), X-Ray Diffraction (XRD), and Fourier Transform Infrared Spectroscopy (FTIR).

Geology and Stratigraphy

The Niger Delta Basin, situated in southern Nigeria, is one of the world's largest delta systems and a prolific hydrocarbon province. The Niger Delta Basin is situated in equatorial West Africa, between latitudes 3°N and 6°N and longitudes 5°E and 8°E. It is located on the continental coast of the Gulf of Guinea (Fig. 1). It covers

75,000 km^2 and is completely filled with clastic sediment that is up to 12,000 m thick (Reijers *et al.* 1997). The basin's evolution was driven by complex interactions between tectonics and sedimentation, resulting in extensive deltaic sequences and multiple oil and gas accumulations. The delta has experienced significant subsidence, creating thick sedimentary sequences that are crucial for hydrocarbon maturation and trapping. The tectonic setting of the Niger Delta basin is influenced by the movements along the equatorial Atlantic oceanic fracture zones that extend beneath the delta and determined the initial locus into which the proto-Niger built its delta. The Benue trough, a NE-SW folded rift basin that runs diagonally across Nigeria, is a much larger and older tectonic feature that the Niger Delta basin occupies the coastal and oceanward part of. It formed simultaneously with the opening of the Gulf of Guinea and the equatorial Atlantic in Aptian-Albian times when Africa and South America began to separate (Short and Stauble, 1967). The Niger Delta has experienced three depositional cycles, with the third cycle from Eocene to Recent marking the continuous growth of the main Niger delta. The subsurface of the Niger delta is divided into three lithostratigraphic units: the upper sandy Benin Formation, the intervening unit of alternating sandstone and shale named the Agbada Formation, and the lower shaly Akata Formation (Reijers, 2011). These units range in age from early Tertiary to Recent and are related to the present outcrops and environments of deposition (Reijers, 2011; Abiola *et al.*, 2018). The Imo Formation, Ameki, and Ogwashi Formations form the up-dip series of the Niger Delta and constitutes the lateral equivalent of the down-dip Akata and Agbada Formations. Within the inland portion of the Niger Delta Basin, the Imo Formation is the oldest geologic unit. The composition includes blue-grey clay and shale, black shale, and various layers of calcareous sandstone, limestone, and marl (Reyment, 1965). In the eastern region, the Imo Formation unconformably overlies the Nsukka Formation and can be observed at various locations such as Oduenyi village, extending westward through Ndiwo. The Imo Formation is conformably overlain by the Ameki Formation comprising of shale, sandy shale, clay sandstone, and fine-grained fossiliferous sandstone (Reyment, 1965; Arua,1986; Arua and Rao, 1987; Ikegwuonu, 2015). The Ogwashi Formation subsequently overlain the Ameki Formation. The Benin Formation made up of coarse to fine-grained sandstones and gravels, with minor shale intercalations was deposited on the Ameki Formation (Doust and Omatsola, 1990)

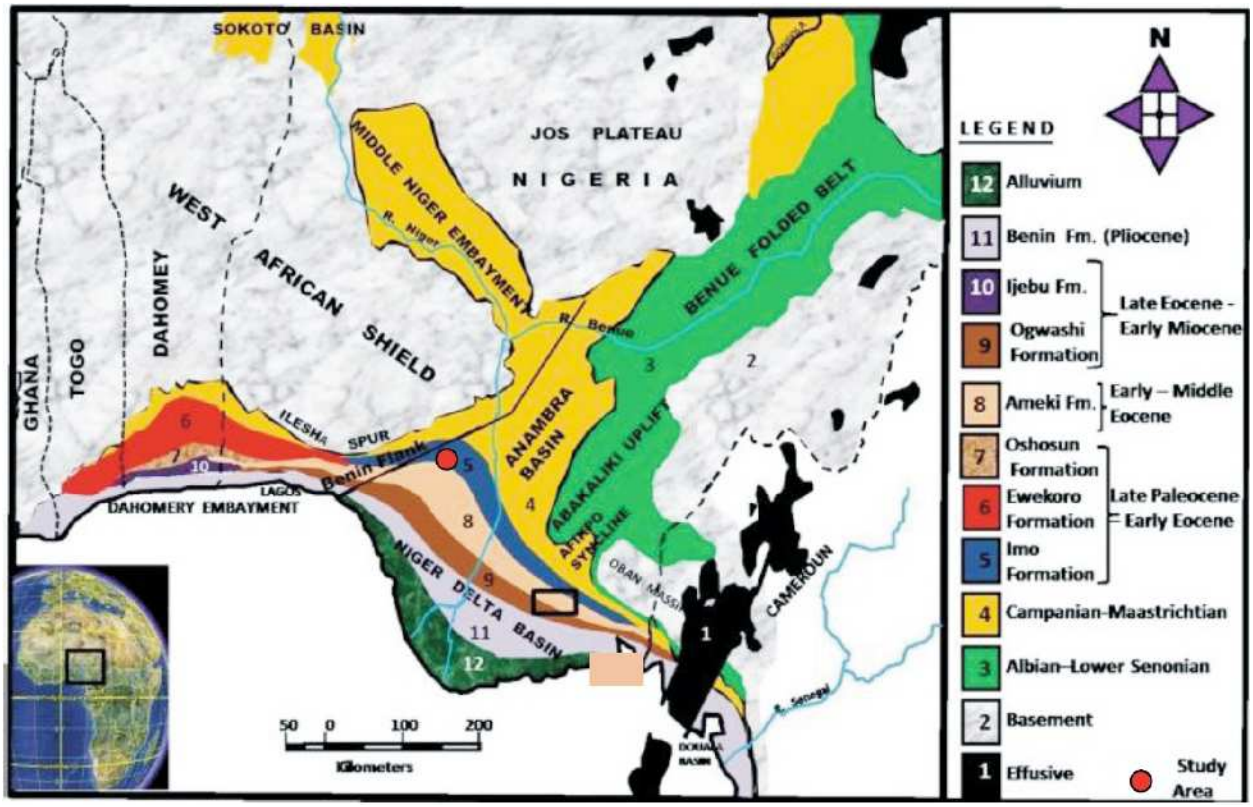


Fig. 1: Geological map of Nigeria showing the Cenozoic succession of the Niger Delta Basin and the location of Owan-1 well (N5° 001 and E5° 451) (modified after Murat, 1972). Fm. = Formation R. = River.

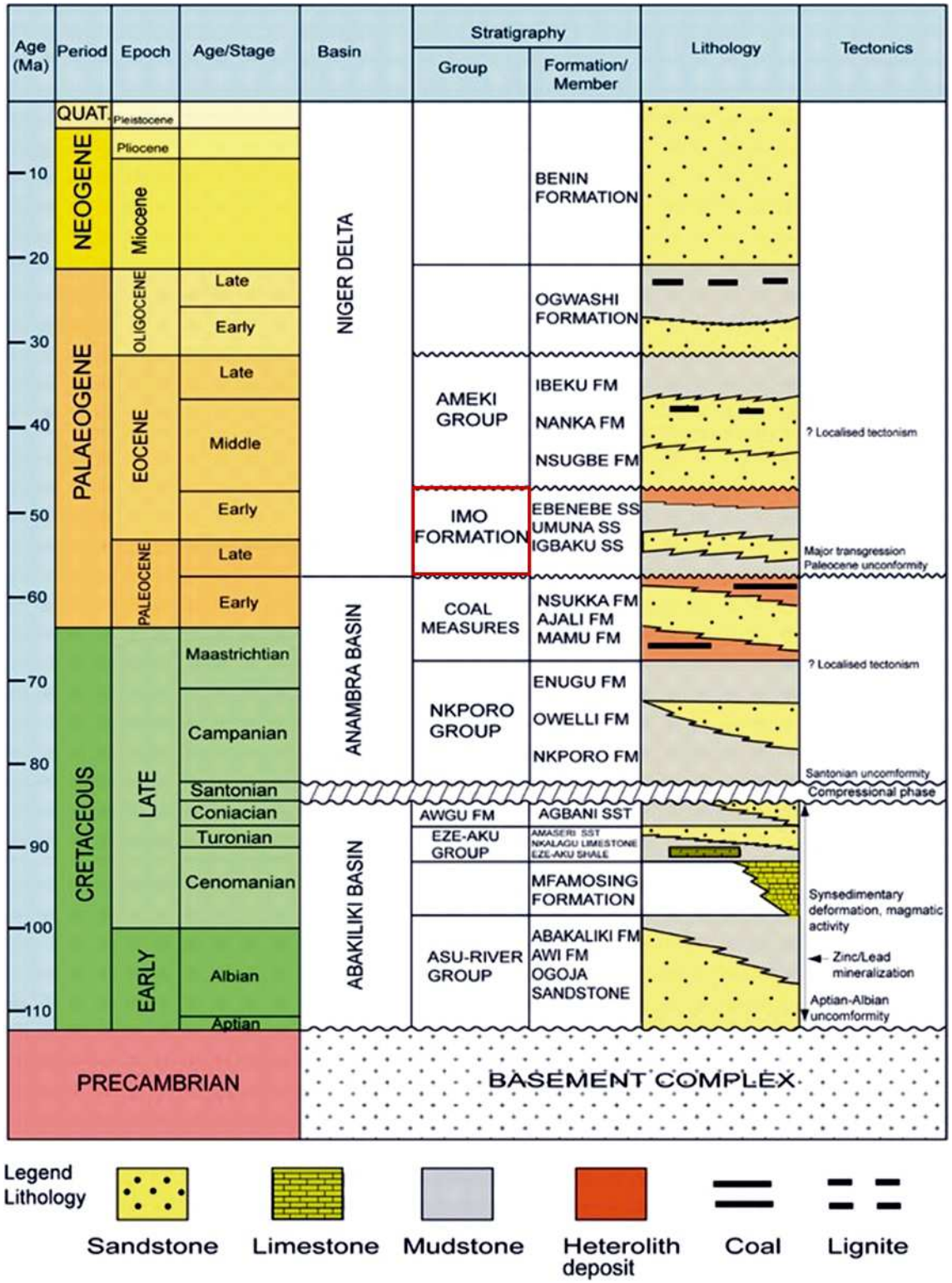


Fig. 2: Stratigraphy of the Benue Trough, Anambra Basin, and the Niger Delta Basin (modified after Ekwenye *et al*. 2016).

Methodology

Twenty-two core samples from Owan-1 well consisting of mainly shales were acquired from the central repository of the Nigerian Geological Survey Agency (NGSA) in Kaduna, Nigeria. The samples were carefully selected at interval between 75 ft-1066 ft (Fig. 3). The total depth of the well is 1746ft which covers the

Maastrichtian Mamu and the Paleocene Imo formations. 13 shale samples were selected and subjected to pulverization prior to laboratory analysis. The laboratory analyses include; XRF, XRD and FTIR. The samples were analyzed by XRF to determine the major elements and some trace elements within the detection limit. The XRD analysis was carried out to determine the mineralogical composition and FTIR to investigate the organic and inorganic compounds present in the shales. The XRF analysis was conducted by XRF machine at Stratochem laboratory in Egypt. The XRD analysis was conducted with a Rigaku D/max-2500/PC powder diffractometer utilizing Ni-filtered Cu-K^3 radiation and a scintillation detector. To eliminate the adsorbed water, the pulverized samples underwent oven-drying at a temperature of 100 °C for a duration of 10 hours. The samples were inserted into rectangular aluminum sample holders manually, using a spatula that had been cleansed with alcohol. The samples were thereafter affixed firmly into the instrument sample container. The samples underwent step scanning within the theta scale range of 5 to 85 degrees, at intervals of 0.02 degrees. Each step was tallied for a duration of 0.5 seconds to ascertain the mineral phases and main

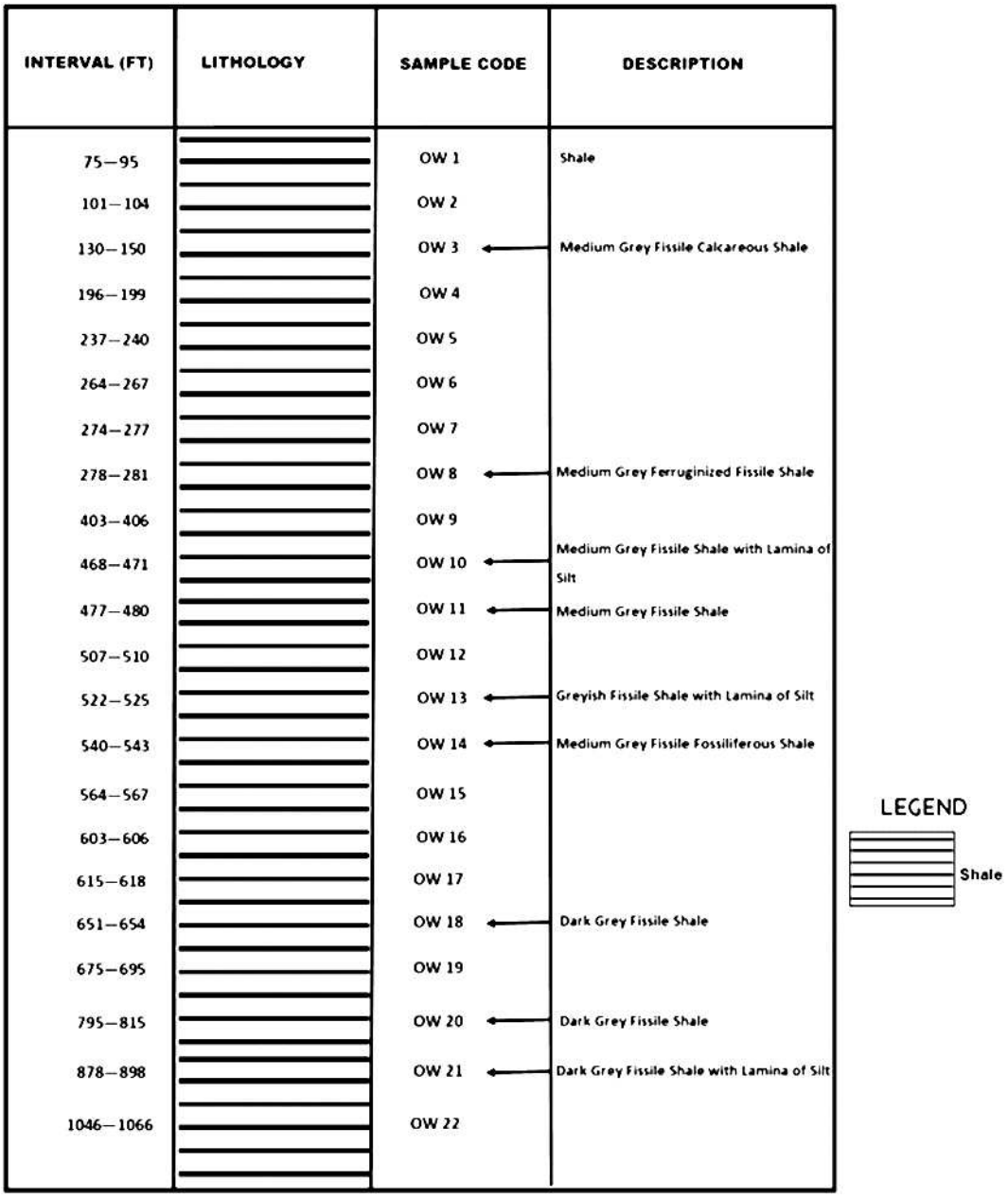


Fig. 3: Lithological succession of Owan-1 well.

elements present in the selected shale samples. A Thermo Nicolet 6700 FTIR spectrometer, complete with the detector and XT-KBr beam splitter, was used for the purpose of conducting FTIR spectroscopy. Pellets were fabricated by grinding 1 mg of crushed shale samples (with a size of 75 mm) with 100 mg of KBr and then pressing them into pellets, following the methodology by Painter *et al.* (1981). The pellets underwent a 48-hour drying process using a vacuum oven to minimize the amount of water in the spectrum. The shale samples were subjected to FTIR spectroscopy using absorbance mode, with a wavelength range of 4000 cm^{1} to 400 cm^{1}. The XRD and FTIR analyses were carried out at Redeemer University, Ede, Osun State Nigeria.

Results and Discussion

Major Elements Geochemistry

The results of the major elements for the shales are presented in Table 1. The geochemical findings were contrasted with established geochemical benchmarks, including the Upper Continental Crust (UCC) as defined by Rudnick and Gao (2003), the North America Shale Composite (NASC) as established by Gromet *et al.* (1984), and the Post Archean Australian shale (PAAS) as described by Taylor and Mclennan (1985) (Table 3 and 4). The primary chemical composition of fine siliciclastic rocks is often determined by clay minerals and non-clay silicate phases (Cox *et al.*, 1995; Moosavirad *et al.*, 2011). Major oxides in the examined shales include P_2O_5, MgO, K_2O, MnO, SiO_2, Al_2O_3, Fe_2O_3, Na_2O, and CaO. The studied shale samples are enriched in SiO_2, Al_2O_3 and Fe_2O_3 compared to CaO, MgO, K_2O, MnO, TiO_2, and P_2O_5 that have low concentrations. SiO_2 is predominant in the samples with concentrations that range between 17.39 wt.% to 30.46 wt. % (average concentration of 25.5 wt. %). Al_2O_3 has concentration ranging from 7.95 wt. % to 11.39 wt. % (average concentration of 9.65 wt. %). Fe_2O_3 has concentration from 2.88–8.69 wt. % (average concentration of 5.46 wt. %). SiO_2, Al_2O_3 and Fe_2O_3 make up about 43.98 wt.% of the major oxides. Generally, there are low concentrations of CaO, MgO, K_2O, MnO, TiO_2 and P_2O_5 (Table 1). The concentration of CaO ranges from 0.45 wt.% to 14.37 wt. % (average 3.21 wt.%) MgO, 0.70 wt.% to 1.45 wt. % (average 0.97 wt.%), K_2O, 1.35wt.% to 1.93 wt. % (average 1.60 wt. %) MnO, 0.00-0.13 wt. % (average 0.05 wt. %), TiO_2, 0.38 wt.% to 1.96 wt. % (average1.05 wt.%) and P_2O_5, 0.73 wt.%-0.99 wt. % (average 0.87 wt%) (Table 1). The relatively low concentration of K_2O indicates the shales are deficient of K-feldspar or illite (Okunlola and Idowu, 2012), and the lack of marine carbonate facies in the sedimentary succession explains the low CaO content (Imeokparia and Onyeobi, 2007).

Table 1: Major elements of the shales in wt%.

Sample Code	SiO_2	Al_2O_3	Fe_2O_3	TiO_2	CaO	K_2O	P_2O_5	MnO	MgO	Na_2O
OW3	27.83	9.36	6.72	1.05	1.98	1.67	0.99	-	0.9	0.6
OW11	21.15	8.18	4.9	0.51	6.01	1.48	0.85	0.06	1.16	0.55
OW12	24.55	9.77	8.69	1.07	0.72	1.85	0.88	0.04	1.45	0.8
OW13	27.1	9.89	5.2	1.17	0.75	1.93	0.88	0.04	1.06	1.1
OW14	17.39	7.95	4.58	0.38	14.37	1.36	0.73	0.13	0.9	1.05
OW18	27.29	9.38	5.5	1.02	0.64	1.79	0.89	-	0.85	0.84
OW20	28.29	11.27	5.19	1.2	0.75	1.35	0.91	-	0.71	0.85
OW21	30.46	11.39	2.88	1.96	0.45	1.38	0.85	-	0.7	0.9
Average	**25.51**	**9.65**	**5.46**	**1.05**	**3.21**	**1.60**	**0.87**	**0.03**	**0.97**	**0.84**

The concentrations of SiO_2, Al_2O_3, Na_2O, MgO, and K_2O in the shale samples are depleted when compared to values of the PAAS, NASC, UCC (Taylor and McLennan, 1985) which suggests that the shale samples may have undergone extensive weathering and multiple cycles of sedimentary recycling as weathering processes typically deplete these elements as they are leached out and transported away from the source area. The Fe_2O_3 of shales is above the values of UCC and relatively close to the value of NASC of the worldwide shales which suggest post depositional diagenesis may have contributed to the iron enrichment (Taylor and McLennan, 1985). TiO_2 values were all higher than values of PAAS, NASC, UCC worldwide shales indicating the source area might have experienced intense weathering and possible presence of resistant minerals like rutile and ilmenite in the shales. The CaO values are less than NASC and UCC value but higher than the PAAS (Table 3).

Table 2: Trace elements composition of the shales in ppm.

Sample ID	V	Zr	Rb	Cr	Zn	Ba	Sr	S	Pb	As	Nb	Cl
OW3	163	172	70	211	118	160	315	7308	15	0	25	161
OW11	0	103	57	191	80	152	299	8103	10	0	13	156
OW12	201	216	76	231	90	292	185	12217	11	17	32	143
OW13	190	251	84	212	85	220	148	2168	18	-	35	143
OW14	0	76	47	182	64	168	304	5198	6	-	8	217
OW18	171	209	76	203	110	157	150	9567	11	16	23	120
OW20	197	204	61	299	130	122	122	10339	23	-	28	183
OW21	194	397	58	161	149	181	203	4160	25	15	43	188
Average	**139.54**	**203.4**	**66.03**	**211.20**	**103.12**	**181.52**	**215.84**	**7382.45**	**14.72**	**6.02**	**25.75**	**168.12**

Table 3: Major oxide of Owan -1 shales compared with worldwide shale.

Major oxide	PAAS	NASC	UCC	Present Study
SiO_2	62.80	64.00	66.00	25.51
Al_2O_3	18.90	16.90	15.20	9.65
Fe_2O_3	7.22	5.65	5.00	5.46
TiO_2	1.00	0.70	0.50	1.05
CaO	1.30	3.63	4.20	3.21
K_2O	3.70	3.97	3.40	1.60
MgO	2.20	2.86	2.20	0.97
Na_2O	1.20	1.4	3.90	0.84
P_2O_5	0.16	0.13	-	0.87

Table 4: Average trace element concentrations compared with other worldwide shale

Trace Elements	PAAS	NASC	UCC	Present study
V	150	130	97	139.54
Zr	210	200	193	203.4
Rb	160	125	82	66.03
Cr	110	125	92	211.20
Zn	85	-	71	103.12
Ba	650	636	628	181.52
Sr	200	142	320	215.84
S	-	-	-	7382.45
Pb	20	-	-	14.72
As	-	28.4	1.50	6.02
Nb	19	13	12	25.75
Cl	-	-	-	168.12

Trace Elements Geochemistry

Tables 2 shows an overview of the concentrations of some trace elements in parts per million (ppm) while Table 6 indicates the ratio of some trace elements. The trace elements identified in the samples include Vanadium (V), Zircon (Zr), Rubidium (Rb), Chromium (Cr), Zinc (Zn), Barium (Ba), Strontium (Sr), Sulphur (S), Lead (Pb), Arsenic (As), Niobium (Nb), and Chlorine (Cl). The average values of these elements are 139.54ppm, 203.4ppm, 66.03ppm, 211.20ppm,103.12ppm, 181.52ppm, 215.84ppm, 7382.45ppm, 14.72ppm, 6.02ppm, 25.75ppm, and 168.12ppm respectively. Sulphur (S) concentration is high in the studied samples ranging from 2168-12217 ppm (average 7382.45 ppm). Elements such as As, Pb, Nb, and Rb have low average concentrations (Table 2). When compared to values of PAAS, NASC and UCC, V and Zr values in the shales are higher than NASC and UCC but less than PAAS. This implies a significant input from mafic or intermediate source rocks, which are typically enriched in these elements (Nesbitt and Young, 1982). High V concentration indicates that the shales likely experienced conditions that favored the retention of V. Cr, Zn and Nb values were above the concentrations of PAAS, NASC and UCC which points to source rocks from mafic compositions (Nesbitt and Young, 1982). Rb and Ba concentrations were less than values of PAAS, NASC and UCC (Table 4). Rb and Ba are relatively mobile during chemical weathering and can be leached out of the sediments. Their depletion suggests that the source area experienced significant weathering and leaching processes (Fedo *et al.* 1996).

Paleoweathering and Paleoclimatic Condition

Clastic sedimentary rocks are thought to have their chemical compositions largely influenced by the weathering and composition of the source area (Nesbitt and Young, 1982; Harnois, 1988; Fedo *et al.* 1996). The process of rock weathering leads to the breakdown of chemical compounds and may cause an increase in Al_2O_3 and a decrease in alkalis such as Na_2O, K_2O, MgO and CaO. The Paleoweathering indices such as Chemical Index of Weathering (CIW), Plagioclase Index of Alteration, (PIA) and Chemical Index of Alteration (CIA) derived from the major element composition, were used to assess the level of weathering

of the source rocks. In this study, the values of CIA for the shales ranged from 32.1% to 80.6% (average 64.0). Similarly, the values of CIW varied between 34.0% and 89.4% (average 71.9) while the PIA ranged from 29.9% - 88.9% (averaging 69.5) (Table 5). The CIA, CIW and PIA values of the shales indicate low to moderate chemical weathering. This observation is shown by the plot of CIA vs Al_2O_3 (Fig. 4).

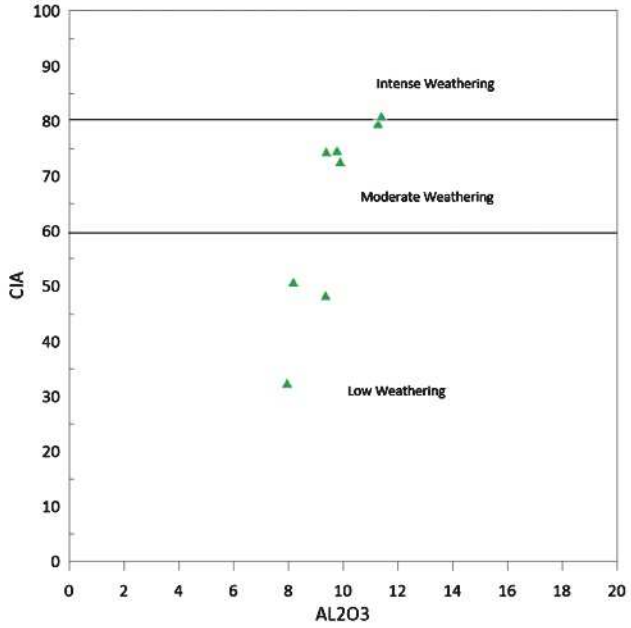


Fig. 4: Bivariate plot of CIA versus Al_2O_3 for the studied shales (after Nesbitt et al, 1980).

Studying paleoclimates aids in comprehending the processes of weathering in the source region as significant elemental signatures offer valuable insights into the paleoclimatic conditions that prevailed during deposition. (Suttner and Dutta, 1986). The CIA provides crucial insights into the paleoclimate conditions that influenced the formation of source rocks. When CIA values are ≤ 50%, it suggest low weathering, 60-80% indicates moderate weathering in a cool and/or arid conditions with limited rainfall, according to studies by Fedo *et al.* (1996). Furthermore, values >80 are linked to hot humid climates with significant alteration of source rocks, as suggested by (Nesbitt and Young, 1982; Fedo *et al.*,1996; McLennan *et al.*, 1993; Kairouani *et al.*, 2023). The average CIA (64%) and CIW (71.9%) values for the shales under investigation suggest a consistent state of weathering in a cool and/or semi-arid-semi-humid climate. This is corroborated by the bivariate plots of Suttner and Dutta (1986) (Figs. 5 and 6). The trace element compositions were also used to constrain the paleoclimatic setting. The Rb/Sr has been used to infer past climatic setting. Low Rb/Sr ratios indicate warm climates and high ratios indicate cold climates; Rb/Sr ratios decrease in dry climates (Chen *et al.*, 1999; Xu *et al.*, 2010). The Rb/Sr ratio ranged from (0.15-0.57) suggesting warm climatic settings (Table 6).

Provenance and Tectonic Settings

Discriminant diagrams based on major and trace elements were used to infer the origin of the shales (Roser and Korsch, 1988; Floyd *et al.*, 1989; McLennan *et al.*, 1993; Verma *et al.*, 2016). The discriminant functions (DF1 and DF2) (Table. 7) were calculated and plotted to unravel the provenance of the shales. All the samples plotted within the intermediate igneous provenance (Fig. 7). According to Garcia *et al.* (1994)

Table 5: Major oxides ratios and paleo weathering indices of the shales

Sample ID	Fe_2O_3 / Al_2O_3	SiO_2 / Al_2O_3	Al_2O_3 / TiO_2	K_2O / Na_2O	Fe_2O_3 + MgO/ k_2O + Na_2O	CIA	CIW	PIA
OW3	0.72	2.97	8.91	2.78	3.36	48.0	52.5	47.6
OW11	0.60	2.59	16.04	2.69	2.99	50.4	55.5	50.5
OW12	0.89	2.51	9.13	2.31	3.83	74.4	86.5	88.9
OW13	0.53	2.74	8.45	1.75	2.07	72.3	84.2	81.1
OW14	0.58	2.19	20.92	1.30	2.27	32.1	34.0	29.9
OW18	0.59	2.91	9.20	2.13	2.41	74.2	86.4	83.7
OW20	0.46	2.51	9.39	1.59	2.68	79.3	87.6	86.1
OW21	0.25	2.67	5.81	1.53	1.57	80.6	89.4	88.1
Average	**0.58**	**2.64**	**10.98**	**2.10**	**2.65**	**64.0**	**71.9**	**69.5**

CIA - Chemical Index of Alteration= [Al_2O_3/ (Al_2O_3+CaO* Na_2O + K_2O)] *100
CIW- Chemical Index of Weathering = [Al_2O_3/(Al_2O_3+CaO+Na_2O)] *100
PIA – Plagioclase Index of Alteration = 100* (Al_2O_3–K_2O) / (Al_2O_3+CaO* Na_2O -K_2O)

Table 6: Trace elements ratios of the shale samples.

SAMPLE	Sr/Ba	Rb/Sr	V/Cr
OW3 Shale	1.97	0.22	0.77
OW11 Shale	1.96	0.19	0.93
OW12 Shale	0.63	0.41	0.87
OW13 Shale	0.67	0.57	0.90
OW14 Shale	1.82	0.15	1.02
OW18 Shale	0.96	0.51	0.84
OW20 Shale	1.00	0.50	0.66
OW21 Shale	1.12	0.28	1.21
AVERAGE	**1.27**	**0.35**	**0.90**

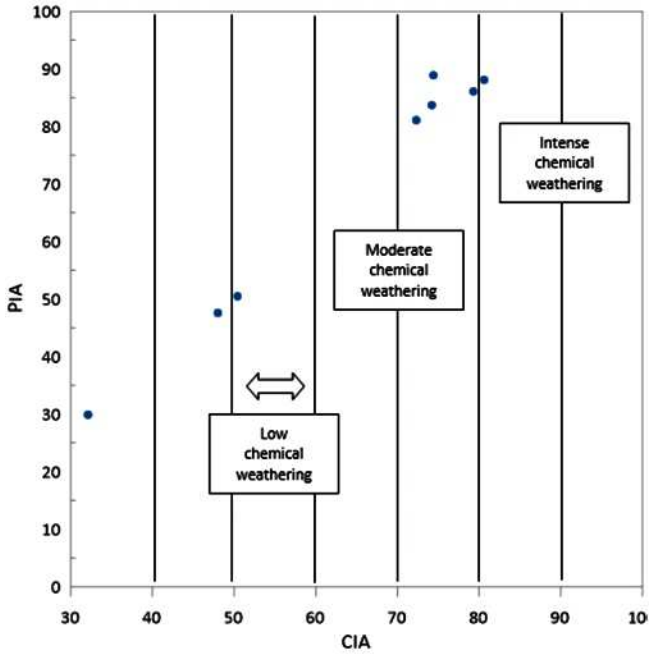


Fig. 5: Paleoweathering plot of CIA versus PIA indicating low to moderate chemical weathering. (after Suttner & Dutta, 1986).

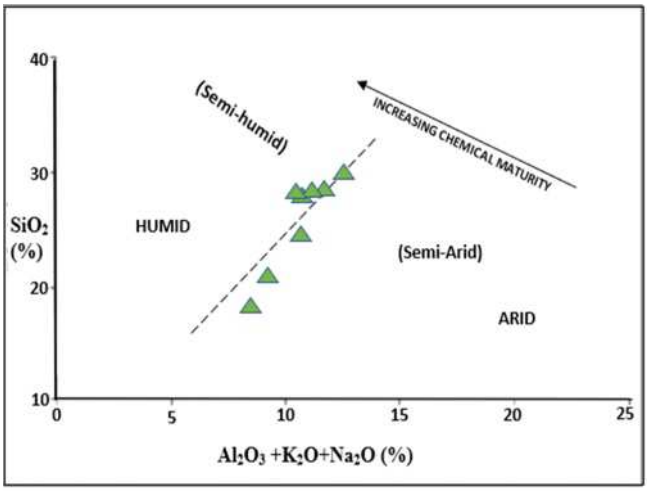


Fig. 6: A bivariate plot of SiO2 vs (Al2O3+ K2O+Na2O) (after Suttner & Dutta, 1986).

and Hayashi *et al.* (2007), the Al_2O_3/TiO_2 in sedimentary rocks are considered a strong indicator of the composition of the source with the following range of values 3–8, 8–21, and 21–70 depicting mafic, intermediate, and felsic sources respectively. The Al_2O_3/TiO_2 in the shales ranged from 5.81 to 20.92 (average 10.98) indicating intermediate igneous provenance (Table 5). However, sample OW20 with value of 5.81 suggest mafic source (Fig. 8). The average of Zr/TiO_2 for the shales is 194.95 which falls within the range of intermediate provenance according to Hayashi et al (1997). This inference is corroborated by the bivariate plot of Zr vs TiO_2 (Fig. 9) after Hayashi *et al.* (2007). Roser and Korsch (1986) proposed a tectonic discriminant diagram by plotting SiO_2 against K_2O/Na_2O. The shale samples were deposited in a passive margin tectonic setting with a few samples plotted in the oceanic island arc and active continental margin (Fig. 10).

Table 7: Discriminant Functions by major element ratio

S/N	Sample code	DF1	DF2
1	OW3	-4.16	-0.76
2	OW11	-3.73	-0.86
3	OW12	-5.40	-1.13
4	OW13	-0.32	1.95
5	OW14	-3.67	-2.77
6	OW18	-1.91	0.31
7	OW20	-3.29	-0.02
8	OW21	1.41	5.90

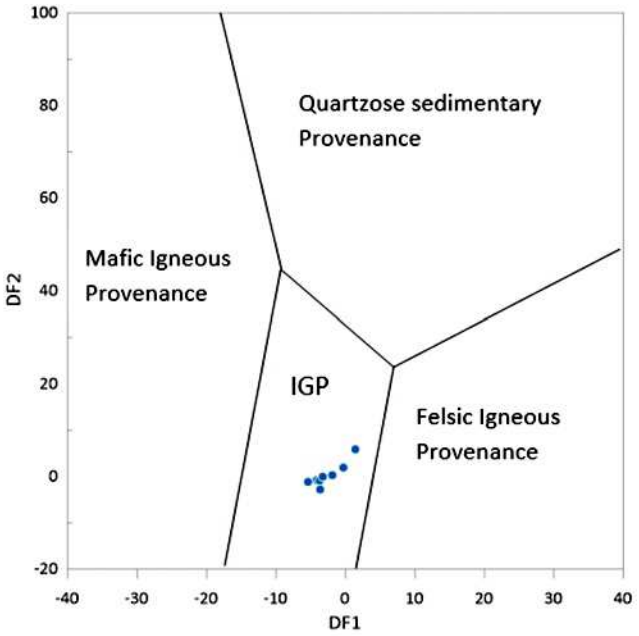


Fig. 7: DF1 vs DF2 Discriminant plot for provenance lithology (after Roser and Korch, 1988).

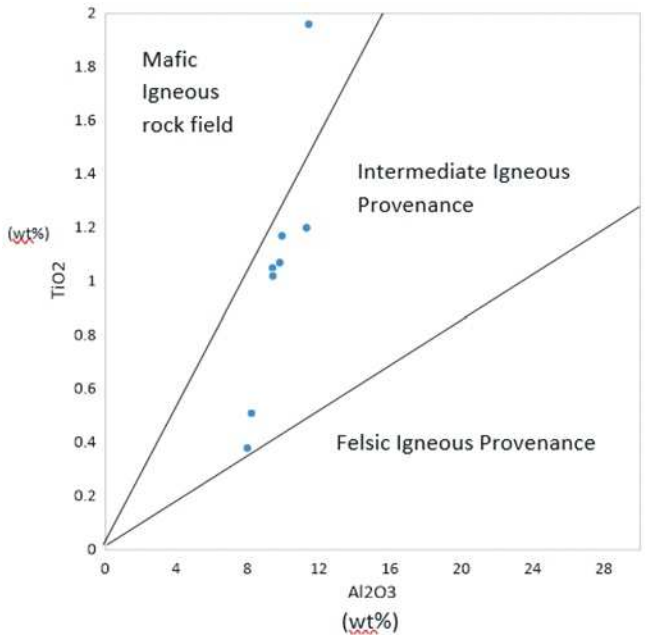


Fig. 8: TiO_2 vs Al_2O_3 Provenance plot for shales of Owan-1 well (Hayashi *et al,* 2007).

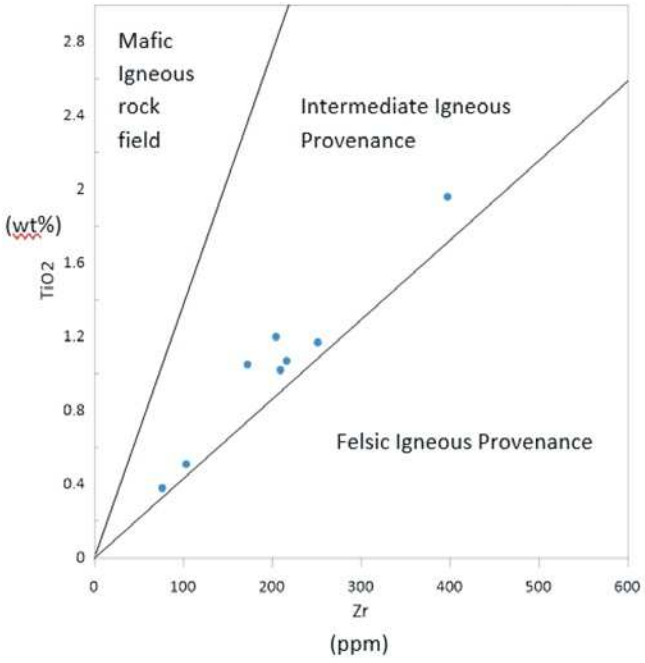


Fig. 9: TiO_2 vs Zr Provenance plot for shales from Owan- 1 well (after Krzeszowska, 2019).

Paleaeoredox and Paleoenvironments

Trace elements composition in sedimentary rocks are important to understanding the palaeoredox condition due to low mobility and residence time in sea water. Hence, elements that are sensitive to redox reactions such as Cr, V, Th, Mo, Ni, Co, U, and Mn are valuable for reconstructing palaeo-redox conditions according to

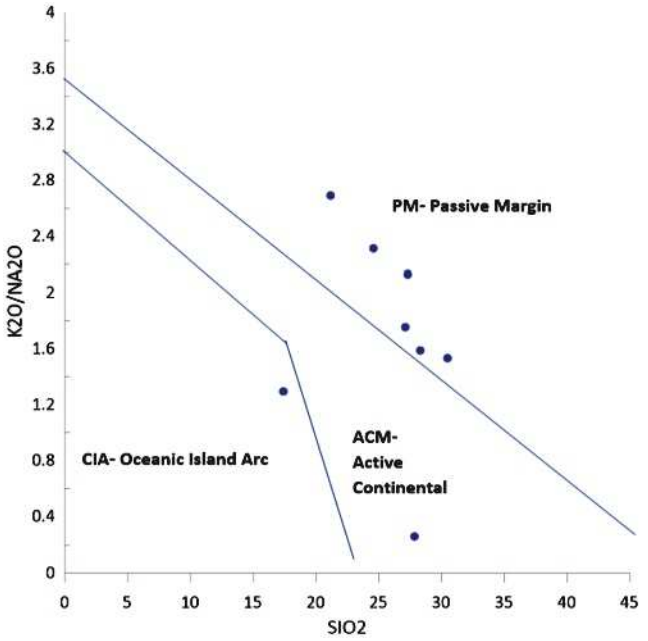


Fig. 10: SiO_2 vs K_2O/Na_2O Provenance tectonic setting plot for shales in the Owan-1 well (after Roser and Korsch, 1986).

(Jones and Manning, 1994; Nath *et al.*, 1997). The Sr/Ba ratio is widely utilized for assessing variations in salinity within sedimentary rocks. The water bodies may be classified into three categories based on their salinity levels: freshwater (salinity <0.5), brackish water (salinity between 0.5 and 1), and saltwater (salinity >1) (Liu, 1980; Wang *et al.*, 2005; Ye *et al.*, 2008). Sr/Ba value greater than 1 indicates deposition in marine setting whereas Sr/Ba value < 1 suggests continental deposition. The Sr/Ba ratio of shales is between 0.62 to 1.97 with an average value of 1.27 (Table 6), indicating marine deposition and high salinity stratification in the water column. The study conducted by Jones and Manning (1994) used the ratio of V/Cr as a means to deduce the redox conditions of mudstones. They found that values < 2 imply oxic condition, 2- 4.25 indicate dysoxic, and > 4.25 indicate suboxic -anoxic condition. The V/Cr in the shales ranged between 0.66-1.21 (Table 6) (average 0.90) therefore denoting oxic depositional condition. Also, the paleodepositional environments of the shales can be inferred through the plot of vanadium against the percentage of Al_2O_3. Majority of the shale samples plotted within the deep marine while few plotted within shallow marine and fluvial environment (Fig. 11).

Kerogen Characterization and Mineralogy from FTIR

FTIR analysis was conducted on ten shale samples to uncover the distinct absorbance bands of organic (hydrocarbon) and mineral contents across the different

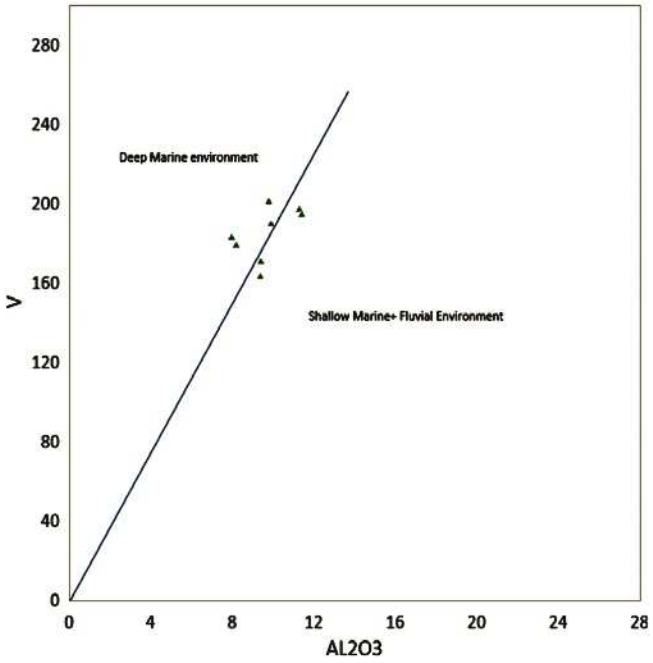


Fig. 11: Cross plots of Vanadium vs Al_2O_3 for the shales of Owan-1 well.

diagnostic wavelengths of the infrared spectrum. The spectrum appearances indicate that the shale samples have complex organic compounds such as saturated and unsaturated alkanes due to high number of absorbance bands (Fig.12 - Fig.21). A broad absorption band between 3650 and 3250 cm^{-1}, suggests hydrogen bond in the samples (Chen *et al.*, 2012). These bands confirmed the presence of hydrates, hydroxyl, and ammonium in the shales. However, the identification of spectra within the frequency ranges of 800–600 cm^{-1}, 1200–1000cm^{-1}, and 1600–1300cm^{-1}provides evidence of the presence of hydroxyl compounds in the shales (Mastalerz & Marc Bustin, 1993; Chen, et al 2012; Liu, *et al.*, 2019; Pejcic *et al.*, 2021). The presence of narrow bands was observed in some samples close to 3670cm^{-1}, and 3550cm^{-1} frequencies indicating presence of phenol. The majority of the analyzed samples display a prominent absorbance peak in the range of 650-900cm^{-1}, which corresponds to the aromatic phenolic group C=C-OH (Tanykova, *et al.*, 2021). The long chain aliphatic (saturated) compound was observed in sample OW14 due to broad band at 1431cm^{-1} plus methylene rocking vibration at band 725 cm^{-1}. The saturated aliphatic C-H stretch vibration for sample OW14 occur in frequency of 2885 cm^{-1} indicating aliphatic methyne C-H. The methyl (CH_3) and methylene (CH_2) C-H bend of saturated alkane are also evident from the bands within 1470-1430 cm^{-1} and 1485-1445 cm^{-1} respectively for most of the samples (Tanykova, *et al.*, 2021) (Fig.12-Fig.21). Also, there was vibrations between the bands of 1680-1620 cm^{-1} confirming unsaturated alkenyl C=C stretch. However, there was no sharp peak at 1850-1630 cm^{-1} to indicate presence of carbonyl C=O group. The presence of cyclohexane was evident in the samples from the band between 1055-1000 cm^{-1}/1005-925 cm^{-1} as well as aromatic C-H in plane bend at 1225-950cm^{-1}. The spectra also showed presence of mono substituted aromatic ring (phenyl) in all the samples within the bands of 770-730 cm^{-1} + 710-690 cm^{-1} while few samples exhibited 1, 3-disubstituted aromatics (ortho). The relative intensities of the peaks corresponding to different types of bonds can provide valuable insights into the types of kerogen and any changes in its composition and maturation levels. These ratios, known as the A factor and C factor, have been extensively studied by Ganz and Robinson (1985) and Ganz (1986). The A and C factors (Table 8) were obtained to characterize the kerogen in the samples; the plot indicated Type II Kerogen from marine phytoplankton and zooplanktons (Fig. 22). Hence, the organic matter was deposited in marine environment which has the potential to generate oil.

A band in the range of 1200 - 900 cm^{-1} was seen in samples OW10, which is attributed to the Si-O bond originating from the silicates (SiO_4^{2-}). The identification of bands at about 1008 cm^{-1}, 779cm^{-1}, 694cm^{-1}, and 468cm^{-1} indicated that the sample OW10 is quartz-rich (Tanykova, *et al.*, 2021). Several different vibration modes at 468cm^{-1} (Si-O bending, Si-O-Fe stretching), 694cm^{-1} (Si-O stretching, Si-O-Al stretching), 914cm^{-1} (Al_2OH bending band of Kaolinite vibration), and at 1033cm^{-1} (Si-O-Si and Si-O stretching) indicates presence of quartz, kaolinite and some illites (Jozanikohan & Abarghooei, 2022). The spectra in the samples reveal bands within 1111cm^{-1}, 1102 cm^{-1} and 1033 cm^{-1} suggesting presence of quartz and clay minerals (Tanykova, *et al.*, 2021).

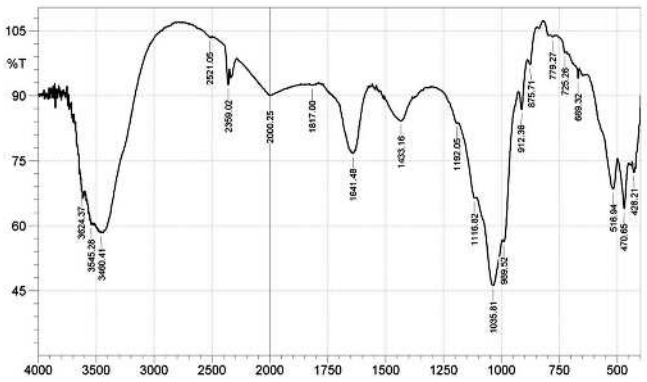


Fig. 12: FTIR Spectra for sample OW2

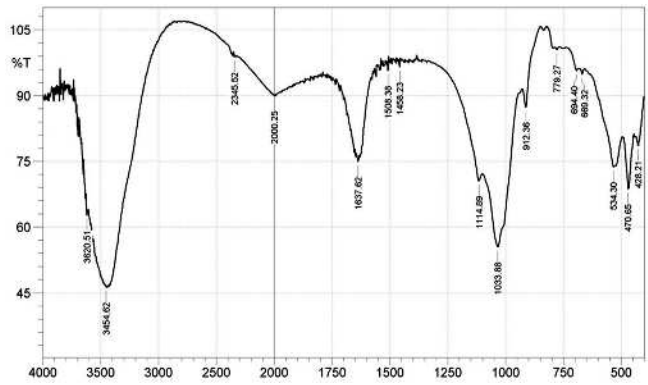


Fig. 13: FTIR Spectra for sample OW3

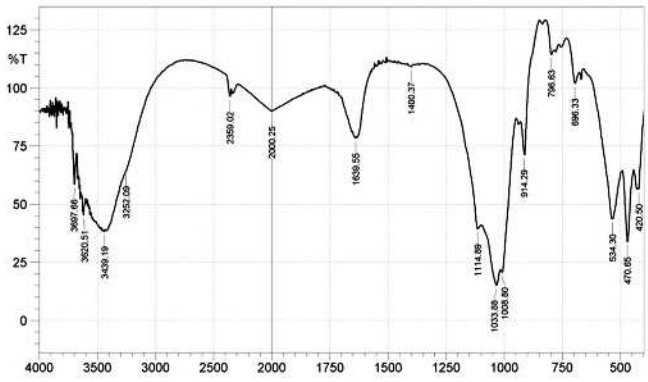


Fig. 14: FTIR Spectra for sample OW4

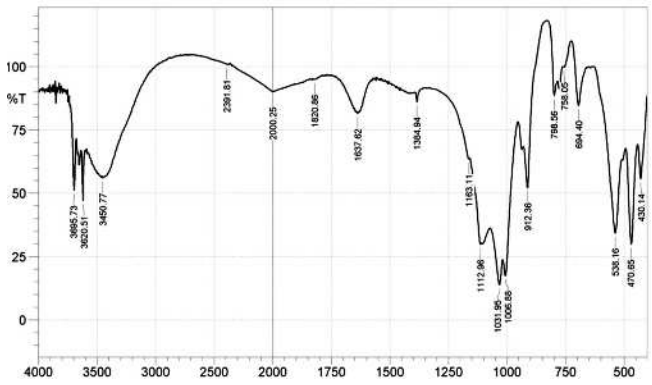


Fig. 15: FTIR Spectra for sample OW8

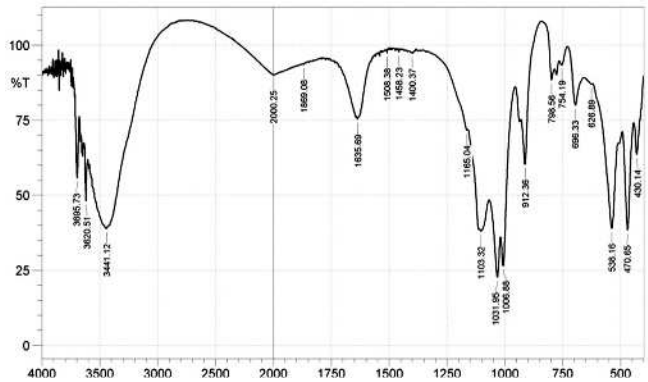


Fig. 16: FTIR Spectra for sample OW9

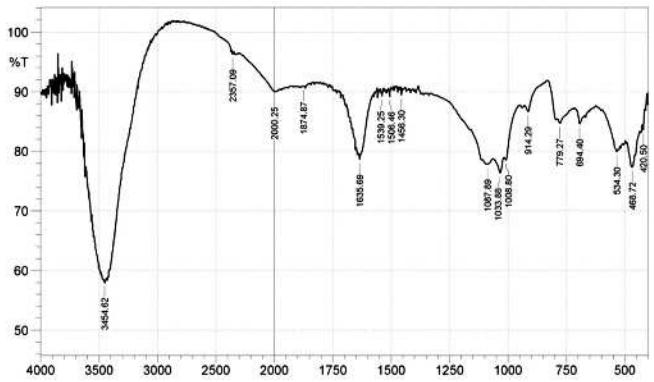


Fig. 17: FTIR Spectra for sample OW10

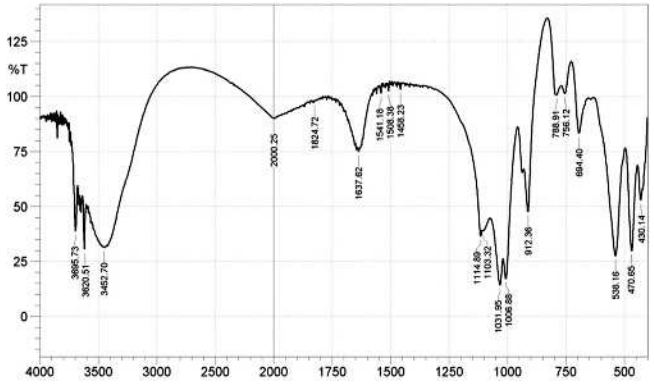


Fig. 18: FTIR Spectra for sample OW11

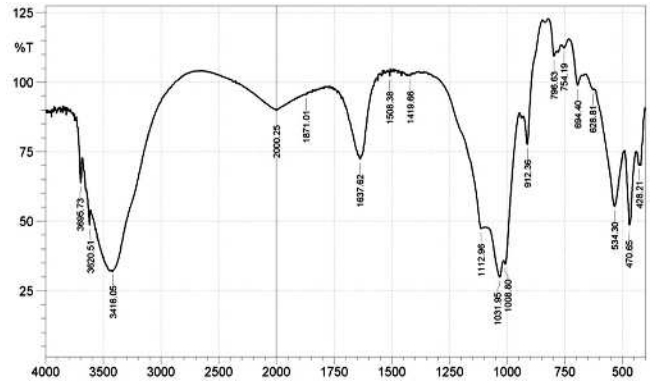


Fig. 19: FTIR Spectra for sample OW12

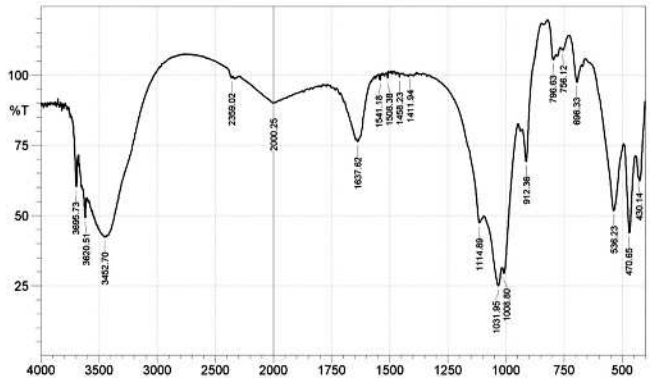


Fig. 20: FTIR Spectra for sample OW13

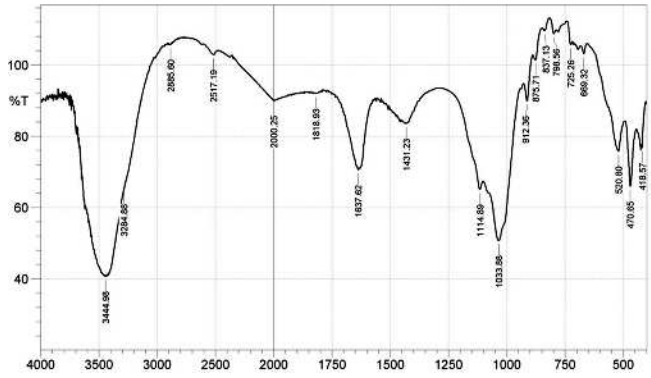


Fig. 21: FTIR Spectra for sample OW14

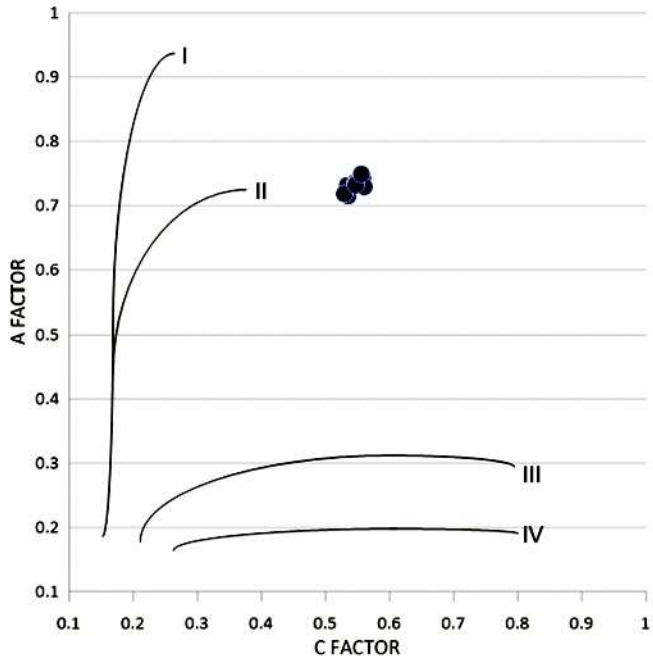


Fig. 22: Classification of Kerogen based on A and C Factors.

Mineralogical Composition

From the XRD results (Table 9), it was observed that the sample OW10 contained the following mineral assemblages; quartz (63%), kaolinite (35%), albite (0.3%), montmorillonite (0.06%), chlorite (1.42%), dolomite (0.02%) and biotite (0.2%). Sample OW8 contained quartz (63%), kaolinite (21%), chlorite (4%), illite (3.5%), montmorillonite (5.5%), biotite (0.5%) and albite (2.5%). The diffractograms are shown in figures 23 and 24. The average values of the minerals are quartz (63%), and kaolinite (28%), montmorillonite (2.78%), chlorite (2.71%). Minor concentration of illite, biotite and carbonates probably mineral (identified as dolomite) were observed in the samples. Kaolinite in the samples are of detrital origin and can be attributed to the strong leaching condition prevailed during tropical warm humid climate. McLennan *et al.*, (1993) had proposed tropical climate interrupted by dry season for the environment with high percentage of Kaolinite. The average composition of kaolinite in the shales confirmed semi-arid to humid climatic condition interrupted by dry season. Furthermore, the average composition of quartz substantiates moderate weathering of the source area. The identification of these minerals through XRD corroborates the inferences from FTIR.

Conclusions

The Paleocene Imo shales of the Niger Delta basin was investigated in this study. The elemental and mineralogical compositions were used to unravel the paleoweathering, paleoredox condition, provenance, tectonic settings and paleoclimatic condition of the

Table 8: A and C factor based on (Ganz and Robinson, 1985; Ganz, 1986)

Sample code	2930 cm^{-1}	2860 cm^{-1}	1630 cm^{-1}	1710 cm^{-1}	A FACTOR	C FACTOR
OW2	105.027	106.161	77.551	88.736	0.73	0.53
OW3	105.613	106.934	76.012	91.568	0.74	0.55
OW4	107.339	110.134	79.140	96.880	0.73	0.55
OW8	102.167	103.591	82.108	94.360	0.71	0.53
OW9	105.625	107.361	76.190	92.711	0.74	0.55
OW10	101.236	101.825	79.656	89.522	0.72	0.53
OW11	109.462	111.666	76.588	96.606	0.74	0.56
OW12	97.462	100.622	73.585	93.709	0.73	0.56
OW13	104.604	106.558	77.494	93.455	0.73	0.55
OW14	105.609	106.452	71.032	88.795	0.75	0.56

Note: $\text{A Factor} = \frac{2930cm^{-1} + 2860cm^{-1}}{2930cm^{-1} + 2860cm^{-1} + 1630cm^{-1}}$ $\text{C Factor} = \frac{1710cm^{-1}}{1710cm^{-1} + 1630cm^{-1}}$

Table 9: Percentage composition of the minerals in the shale samples.

Code	Lithology	Quartz (%)	Kaolinite (%)	Illite (%)	Montmorillonite (%)	Chlorite (%)	Albite (%)	Biotite (%)	Dolomite (%)	Total
OW10	Shale	63	35	-	0.06	1.42	0.3	0.2	0.02	100
OW8	Shale	63	21	3.5	5.5	4	2.5	0.5	-	100
	Avg.	63	28	-	2.78	2.71	1.4	0.35	-	

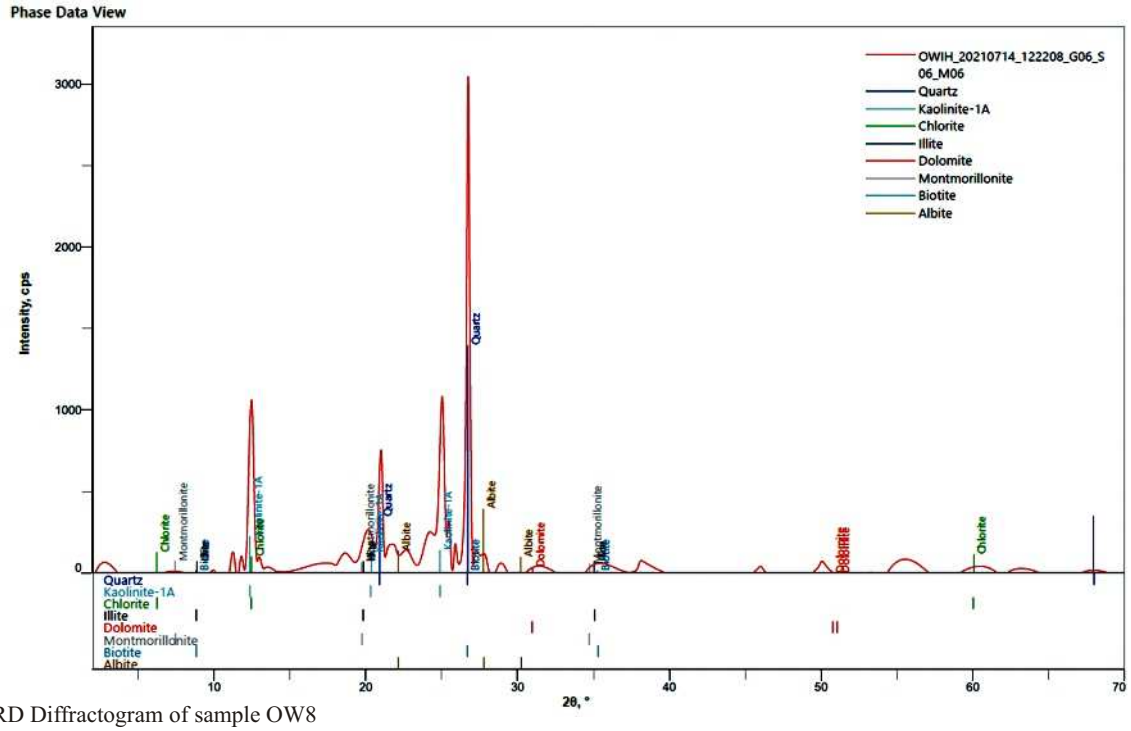


Fig. 23: XRD Diffractogram of sample OW8

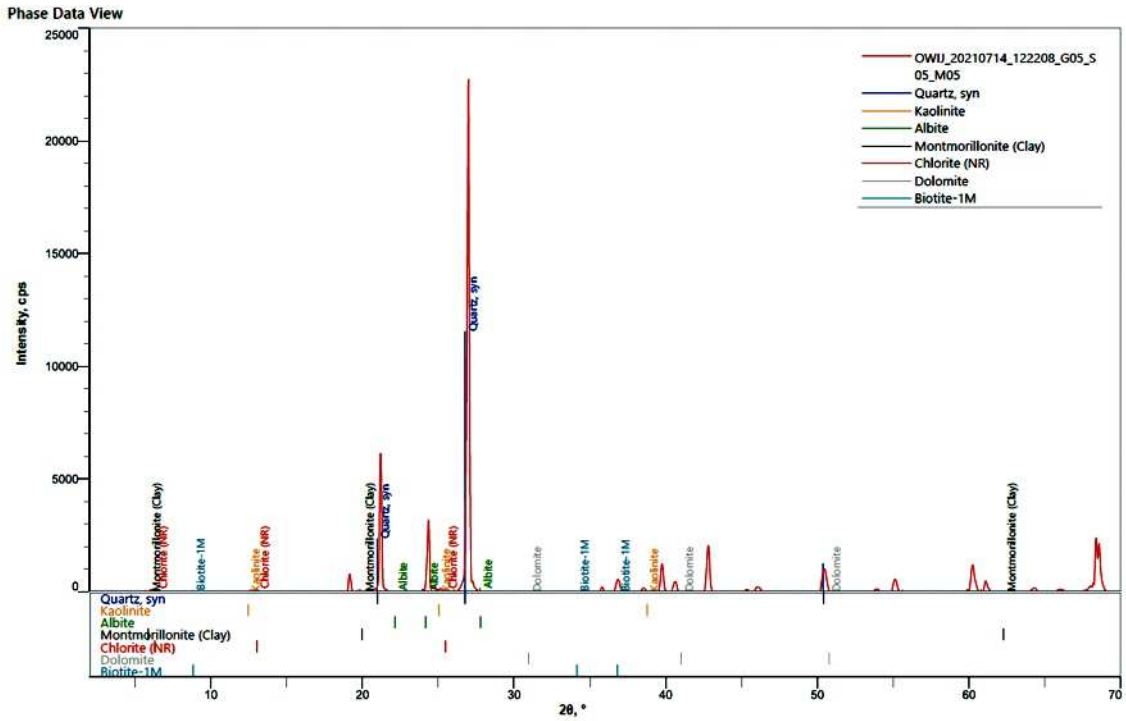


Fig. 24: XRD Diffractogram of sample OW10

provenance area. The average SiO_2 and Al_2O_3 concentrations for the shales are (25.51% and 9.65%) respectively confirming influx of detrital and argillaceous sediments in the area. The high Sr/Ba also indicated meteoric diagenesis as well as high stratification of the water column. The Sr/Ba value >1 (avg. 1.27) suggests mainly marine depositional environments under oxic setting. The bivariate plots of the weathering indices suggested low to moderate weathering. This is supported by the presence of kaolinite (avg. 28%) thus confirming semi-arid to semi-humid paleoclimatic conditions. The discriminants plot (DF1 vs DF2) and bivariate plots of (Zr vs Al_2O_3) indicated intermediate igneous provenance. The shales were mainly deposited under passive margin tectonic setting. The FTIR revealed organic and mineralogical composition of the shales. A broad absorption bands, suggests complex organic compounds such as saturate, aromatic, hydroxyl and phenolic. The spectra in the samples revealed bands within 1111cm^{-1}, 1102cm^{-1} and 1033cm^{-1} suggesting presence of quartz, kaolinite and illite. The characterization of the kerogen through FTIR shows occurrence of Type II kerogen.

Declarations

Conflict of Interest

The authors confirm that they have no identified personal ties or conflicting financial interests that might have had an impact on the research provided in this publication.

Acknowledgements

The authors thank the Nigeria Geological Survey Agency (NGSA) for releasing the core samples for the research.

References

Abiola, O. Olowokere, M. & Ojo, J. (2018). Sequence stratigraphy and depositional sequence interpretation: A case study of "George" Field, offshore Niger Delta, Nigeria. Petroleum Research, 3(1), 25–32.

Adegoke, O. Ladipo, K. Bako, M. & Umaru, A. (2015). Nigeria's Frontier Basins - Unrealized Rift System Hydrocarbon Potential. Petroleum Systems in "Rift" Basins, 651–710.

Aigbadon, G. O. Odoma, A. N. Obasi, I. A. Christopher, S. D., Nanfa, C. A., Aminu, M. B., & Akakuru, O. C. (2022). Hydrocarbon prospectivity of the southern Bida and northern Anambra basins, Nigeria using palynological and geochemical studies. Geosystems and Geoenvironment, 1(4), 100-103.

Arua, I. (1986). Paleoenvironment of Eocene Ameki Formation of the Afikpo syncline, southern Nigeria. Journal of African Earth Sciences 5, 279–284.

Arua, I., and Rao, V. R. (1987). New stratigraphic data on the Eocene Ameki Formation, southeastern Nigeria. Journal of African Earth Sciences 6, 391–397.

Bustin, R. M. (1988). Sedimentology and Characteristics of Dispersed Organic Matter in Tertiary Niger Delta: Origin of Source Rocks in a Deltaic Environment. AAPG Bulletin, 72 (3), 277–298.

Chen, J., An, Z., Head, J. (1999). Variation of Rb/Sr ratios in the Loess-paleosol sequences of central China during the last 130,000 years and their implications for Monsoon Paleoclimatology. Quat. Res. 51, 215–219.

Chen, Y. Mastalerz, M. & Schimmelmann, A. (2012). Characterization of chemical functional groups in macerals across different coal ranks via micro-FTIR spectroscopy. International Journal of Coal Geology, 104, 22-33.

Chudi, O. K. Lewis, H. Stow, D. A. V. & Buckman, J. O. (2016). Reservoir quality prediction of deep-water Oligocene sandstones from the west Niger Delta by integrated petrological, petrophysical and basin modelling. Geological Society, London, Special Publications, 435(1), 245–264.

Cox, R. Low, D. R. Cullers, R. L. (1995). The influence of sediment recycling and basement composition on evolution of mudrock chemistry in the southwestern United States. Geochem. Cosmochim. Acta 59, 2919–2940.

Dim, C. I. P. Onuoha K. M. Okeugo C. G. Ozumba, B. M. (2017). Petroleum system elements within the Late Cretaceous and early Paleogene sediments of Nigeria's inland basins: an integrated sequence stratigraphic approach. Journal of African Earth Science 130:76–86.

Doust, H. and Omatsola, M. E. (1990). The Niger Delta: Hydrocarbon potential of a major Tertiary delta province, Proceeding of KNGMG Symposium "Coastal Lowland Geology and Geotechnology" 1987, 203–212. Dordrecht: Kliwer.

Edegbai, A. J. Schwark, L. Oboh-Ikuenobe, F. E. (2019). Campano-Maastrichtian paleoenvironment, paleotectonics and sediment provenance of western

Anambra Basin, Nigeria: multi-proxy evidences from the Mamu Formation. Journal of African Earth Science. 156, 203–239.

Ejeh, O. I., Etobro, I. A. A. Perleros, K. Ogala, J. E. Ehinola, A. O. Christanis, K. & Kalaitzidis, S. (2024). Hydrocarbon generation potential of Campano-Maastrichtian to Paleogene shales in the Benin Flank of the Anambra Basin, SW Nigeria. Energy Geoscience, 5(3), 1-14.

Ekwenye O. C. Nichols, G. J. Okogbue, C. O. Mode, A. W. (2016). Trace fossil assemblages in the tide-dominated estuarine system: Ameki Group, south-eastern Nigeria. Journal of African Earth Sciences, 118:284-300.

Fedo, C. M. Eriksson, K. Krogstad, E. J. (1996). Geochemistry of shale from the Archean (~3.0 Ga) Buhwa Greenstone belt, Zimbabwe: implications for provenance and source area weathering. Geochem. Cosmochim. Acta 60, 1751–1763.

Floyd, P. Winchester, J. & Park, R. (1989). Geochemistry and tectonic setting of Lewisian clastic metasediments from the Early Proterozoic Loch Maree Group of Gairloch, NW Scotland. Precambrian Research, 45(1–3), 203–214.

Ganz, H. (1986). Organisch und anorganisch geochemische Untersuchungen an figyptischenSchwarzschiefer/Phosphoritsequenzen -Methodenentwicklung und genetisches Modell. Berliner geowissenschaftliche Abhandlungen, A70. Verlag von Dietrich Reimer, Berlin, 113 pp.

Ganz, H. and Robinson, V. (1985). Newly developed infrared method for characterizing kerogen Type and Thermal Maturation. 12th International Meeting on Organie Geochemistry, Abstracts. Jfilich, W. Germany, p. 94.

Garcia, D. Fonteilles, M. Moutte, J. (1994). Sedimentary fractionations between Al, Ti, and Zr, and the genesis of strongly peraluminous granites. J. Geol. 102, 411–422.

Gromet, L. P. Dymek, R. F. Haskin, L. A. Korotev, R. V. (1984). The North American shale composite: its composition, major and trace element characteristics. Geochem. Cosmochim. Acta 48, 2469–2482.

Harnois, L. (1988). The CIW index: a new chemical index of weathering. Sediment. Geol. 55, 319–322.

Hayashi, K. Fujisawa, H. Holland, H. Ohmoto, H. (1997). Geochemistry of 1.9 Ga sedimentary rocks from northeastern Labrador, Canada. Geochem. Cosmochim. Acta 61, 4115–4137.

Ikegwuonu, O. N. (2015). Middle Paleocene to Early Miocene Palynostratigraphy of sediments in Bende-Umuahia area, Niger Delta, basin, southeastern Nigeria, Unpublished M.Sc. Thesis, Department of Geology, University of Nigeria Nsukka, p. 45.

Ikegwuonu, O. N. Umeji, O. P. Chiaghanam, O. I. Nwozor, K. K. Ndukwe, O. S. & Chiadikobi, K. C. (2020). Palynomorph assemblage biozonation of Paleogene strata in Bende–Umuahia Area, Niger Delta Basin, southeastern Nigeria. Journal of Palaeogeography, 9(13), 1-13.

Imeokparia, E. G. and Onyeobi, T. U. (2008). Geochemistry and depositional characteristics of Maastrichtian shales in parts of Southwestern Nigeria. Journal of Mining and Geology, 43(2), 167-174.

Jones, B. Manning, D. A. C. (1994). Comparison of geochemical indices used for the interpretation of paleoredox conditions in ancient mudstones. Chem. Geol. 114, 111–129.

Jozanikohan, G. & Abarghooei, M. N. (2022). The Fourier transform infrared spectroscopy (FTIR) analysis for the clay mineralogy studies in a clastic reservoir. Journal of Petroleum Exploration and Production Technology, 12, 2093 - 2106.

Kairouani, H., Zaghloul, M. N., Abbassi, A. Micheletti, F., Fornelli, A., El Mourabet, M. Critelli, S. (2023). Provenance and source-to-sink of lower-middle Jurassic sediments from hinterland mounts to NW-Gondwana hyper-extended passive margin (Prerif sub-domain, External Rif, Morocco): First evidence from sedimentary petrology and detrital Zircon geochronology. Marine and Petroleum Geology, 157, 106-492.

Krzeszowska, E. (2019). Geochemistry of the Lublin Formation from the Lublin Coal Basin: Implications for weathering intensity, palaeoclimate and provenance. International Journal of Coal Geology, 216, 103-306.

Liu, B. J. (1980). Sedimentary Petrology Geological Press, Beijing pp. 13-89

Liu, B. Schieber, J. & Mastalerz, M. (2019). Petrographic and micro-FTIR study of organic matter in the Upper Devonian new Albany shale during thermal maturation: Implications for kerogen transformation. Memoir 120: Mudstone diagenesis: Research perspectives for shale hydrocarbon reservoirs, seals, and source rocks.

Mastalerz, M. Marc Bustin, R. (1993). Electron microprobe and micro-FTIR analyses applied to maceral chemistry. International Journal of Coal Geology, 24(1–4), 333–345.

McLennan, S. M. Hemming, S. McDaniel, D. K. Hanson, G. M. (1993). Geochemical approaches to sedimentation, provenance, and tectonics. In: Johnsson, M.J., Basu, A. (Eds.), Processes Controlling the Composition of Clastic Sediments, 284. Geological Society of America. Special Papers, 21–40.

Moosavirad, S. Janardhana, M. Sethumadhav, M. Moghadam, M., & Shankara, M. (2011). Geochemistry of lower Jurassic shales of the Shemshak Formation, Kerman Province, Central Iran: Provenance, source weathering and tectonic setting. Geochemistry, 71(3), 279–288.

Murat, R. C. (1972). Stratigraphy and Paleogeography of the Cretaceous and lower tertiary in southern Nigeria. In African geology, ed. T.F.J. Dessauvagie and A.J. Whiteman. Ibadan: University of Ibadan.

Nath, B. N. Bau, M. Ramalingeswara Rao, B. Rao, C. M. (1997). Trace and rare earth elemental variation in Arabian Sea sediments through a transect across the oxygen minimum zone. Geochem. Cosmochim. Acta 61, 2375–2388.

Nesbitt, H. Markovics, G. & price, R. (1980). Chemical processes affecting alkalis and alkaline earths during continental weathering. Geochimica Et Cosmochimica Acta, 44(11), 1659–1666.

Nesbitt, H. W. Young, G. M. (1982). Early Proterozoic climates and plate motions inferred from major element chemistry of lutites. Nature 299, 715–717.

Nesbitt, H. W. Young, G. M. (1984). Prediction of some weathering trends of plutonic and volcanic rocks based on thermodynamic and kinetic considerations. Geochem. Cosmochim. Acta 48 (7), 1523–1534.

Nwajide, C. S. and Reijers, T. J. A. (1996). Geology of the southern Anambra Basin. In: Reijers, T. J. A., (ed). Selected Chapters on Geology. Warri: SPDC, 133-148.

Ogbe, O. B. Orajaka, I. P. Osokpor, J. Omeru, T. & Okunuwadje, S. E. (2020). Interaction between sea-level changes and depositional tectonics: Implications for hydrocarbon prospectivity in the western coastal swamp depobelt, Niger Delta Basin, Nigeria. AAPG Bulletin, 104(3), 477–505.

Okunlola, O. A. Idowu, O. (2012). The geochemistry of claystone-shale deposits from the maastritchian Patti formation, Southern Bida basin, Nigeria. Earth Sciences Research Journal, 16, 139-150.

Omietimi, E. J. Lenhardt, N. Yang, R., Götz, A. E. & Bumby, A. J. (2022). Sedimentary geochemistry of Late Cretaceous-Paleocene deposits at the southwestern margin of the Anambra Basin (Nigeria): Implications for paleoenvironmental reconstructions. Palaeogeography, Palaeoclimatology, Palaeoecology, 600, 111059.

Ozumba, B. M. & Dim, C. I. P. (2022). Biostratigraphy and sequence stratigraphy of the deep offshore Niger Delta and implications for future hydrocarbon exploration in the Paleogene sequences. Interpretation, 10(1), 195–211.

Painter, P. C. Rimmer, S. M. Snyder, R. W. and Davis, A. A. (1981). Fourier transform infrared study of mineral matter in coal: The application of a least squares curve-fitting program. Appl. Spectrosc., 35, 102–106.

Pejcic, B. Shelton, T. le Gras, M. Laukamp, C. Francis, N. Lau, I. (2021). Mid infrared spectral library. Perth: CSIRO:EP2021-1148.

Reijers, T. J. A. (2011). Stratigraphy and sedimentology of the Niger delta. Geologos, 17(3), 133–162.

Reijers, T. J. A. Petters, S. W and Nwajide, C. S. (1997). The Niger Delta Basin. In African basins, ed. R.C. Selley, 151–172. Amsterdam: Elsevier.

Reyment, R. A. (1965). Aspects of the geology of Nigeria—The Stratigraphy of the Cretaceous and Cenozoic Deposits. Ibadan University Press, 133 p.

Roser, B. P. Korsch, R. J. (1986). Determination of tectonic setting of sandstone-mudstone suites using SiO_2 content and K_2O/Na_2O ratio. J. Geol. 94, 635–650.

Roser, B. P. Korsch, R. J. (1988). Provenance signatures of sandstone-mudstone suites determined using discriminant function analysis of major-element data. Chem. Geol. 67, 119–139.

Rudnick, R. L. Gao, S. (2003). Composition of the continental crust. Treatise Geochem. 3, 1–64.

Short, K.C. and Stauble, A. J. (1967). Outline of geology of Niger Delta. AAPG Bulletin 51 (5), 761–779.

Suttner, L. J. Dutta, P. K. (1986). Alluvial sandstone composition and paleoclimate, framework mineralogy. J. Sediment. Petrol. 56 (3), 329–345.

Tanykova, N. Petrova, Y., Kostina, J. Kozlova, E., Leushina, E. & Spasennykh, M. (2021). Study of Organic Matter of Unconventional Reservoirs by IR Spectroscopy and IR Microscopy. Geosciences, 11(7), 277.

Taylor, S. R. McLennan, S. M. (1985). The continental Crust: its Composition and Evolution. Blackwell Scientific Publication, Carlton, p. 312.

Verma, S. P. Díaz-Gonzalez, L. Armstrong-Altrin, J. S. (2016). Application of a new computer program for tectonic discrimination of Cambrian to Holocene clastic sediments Earth. Sci. Inf. 9 (2), 151–165.

Wang, M. F. Jiao, Y. Q. Wang, Z. H. Yang, Q. Yang, S. K. (2005). Recovery paleosalinity in sedimentary environment-An example of mudstone in Shuixigou group, southwestern margin if Turpan-Hami basin Xinjiang. Petrol. Geol., 26 (6)117-120

Xu, H. Liu, B. Wu, F. (2010). Spatial and temporal variations of Rb/Sr ratios of the bulk surface sediments in Lake Qinghai. Geochemical Transactions. 11(3), 1-8.

Ye, L. M. Qi, T. J Peng, H. Y. (2008). Depositional environment analysis of Shanxi Formation in eastern Ordos Basin. Acta Sedimentol. Sin., 26, 202-210.